Available online at www.sciencedirect.com
ScienceDirect
Catalysis Today 126 (2007) 64–72
CATALYSIS TODAY
www.elsevier.com/locate/cattod

Combining diffuse reflectance infrared spectroscopy (DRIFTS), dispersive EXAFS, and mass spectrometry with high time resolution: Potential, limitations, and application to the study of NO interaction with supported Rh catalysts

Mark A. Newton [a,*], Andrew J. Dent [b], Steven G. Fiddy [c], Bhrat Jyoti [d], John Evans [b,d]

[a] *The European Synchrotron Radiation Facility, 6 rue Jules Horowitz, BP220, 38043 Grenoble, France*
[b] *Diamond Light Source, Chilton OX11 0QX, United Kingdom*
[c] *Synchrotron Radiation Source, Daresbury, Warrington, United Kingdom*
[d] *School of Chemistry, University of Southampton, Highfield, Southampton SO17 1BJ, United Kingdom*

Available online 20 November 2006

Abstract

We describe a new experiment that combines transmission based structural probes, such as dispersive EXAFS (EDE), with diffuse reflectance infrared spectroscopy (DRIFTS) and mass spectrometry (MS), at high time resolution. The potential and limitations of this experiment are discussed, and an example of its application to the study of fundamental steps occurring during gas–solid interactions is given; that of oxidation and reduction of alumina supported Rh at 573 K using NO and H_2, and the structural-reactive role of linear ($Rh(NO^+)$) Rh-nitrosyl species within these processes.

Keywords: In situ; Time resolved spectroscopies; DRIFTS; Dispersive EXAFS; Mass spectrometry; QSARS; Rhodium; Nanoparticles; γ-Alumina; NO reduction; Selectivity

1. Introduction

The importance of studying gas–solid or gas–liquid processes in situ and with synchronously applied spectroscopies has become more and more evident [1]. Many important processes within catalysis, chemistry, and materials science involve a complex interplay of fundamental physics and chemistry over a wide range of potential parameter space, length, and timescales.

As such, experiments that can combine, without undue sacrifice, two or more complementary spectroscopies are both highly practical and inherently internally consistent. Such experiments have the potential for the derivation of much sought after, though often elusive, quantitative structure function relationships (QSARS) with a high degree of confidence.

Concomitantly, recent years have seen a wide range of experiments that combine techniques implemented. These range from those techniques that operate on widely differing length scales, such as XRD and EXAFS [2,3], to other multitechnique experiments comprising probes of structure, functionality, and reactivity. Experiments permitting processes to be studied using EXAFS in tandem with, UV–vis [4], UV–vis and Raman [5,6], attenuated total reflection (ATR) infrared [7,8], and mass (MS) spectroscopies have been implemented for studying in situ behaviour of working catalysts at both ambient and high pressures and for both gas–solid and liquid–solid systems.

To this burgeoning canon we have recently added a system for synchronously obtaining EXAFS (in transmission), diffuse reflectance infrared spectroscopy (DRIFTS) and MS [9]. The prime driver for this development lay in the wish to be able to address structure, function, and reactivity in gas–solid interactions in a correlated and dynamic manner. It has become abundantly clear that many structural processes, particularly redox cycles in supported metal catalysts that have direct ramifications for catalysts performance, can occur very rapidly indeed [10–18]. Comprehending them, therefore, requires the application of experiments that can probe structure, function,

* Corresponding author. Tel.: +33 476 88 2809; fax: +33 476 88 2784.
E-mail addresses: newton@esrf.fr, je@soton.ac.uk (M.A. Newton).

0920-5861/$ – see front matter © 2006 Published by Elsevier B.V.
doi:10.1016/j.cattod.2006.09.034

and reactivity with sufficient time resolution to be able to capture the processes themselves, rather than just the states that exist before and after they have occurred.

The weak link in this experimental chain has, arguably, been on the structural side of things. For many years extremely rapid reactor based mass spectrometric study of gas–solid interactions has been possible [19]. From a functional perspective, state of the art FT-IR instruments have also been available for some years that are capable of spectral repetition on the few tens of milliseconds time scale (in a single shot) and beyond (in step scan mode for highly reversible processes) [20].

Though it is clear that diffraction based methodologies can now also be achieved on these sorts of timescales it is the case, especially with many homogeneous and heterogeneous catalysts systems, that the reactive phases are not easily amenable to diffraction based study due to their inherent molecular or disordered/small nature. In these cases, what is ideally required is a time resolving elementally specific probe of local structure.

From a practical point of view, this currently means dispersive EXAFS (EDE), wherein a sample is instantaneously illuminated with the energetic bandwidth required to make an X-ray adsorption (XAFS) measurement [21]. Though the Quick EXAFS technology (where an X-ray monochromator is physically moved to scan through the required energy range) that could fulfil the task of recording changes in local structure on such timescales has been developed and demonstrated for both XANES [11] and EXAFS [22] acquisition, to our knowledge there is currently no permanently available and accessible facility dedicated to this end. By contrast there are several dispersive facilities that are currently active with more planned at new third generation facilities currently under construction.

Dispersive EXAFS does, however, come with its own constraints and considerations [21] and, it would be fair to say that, for all the promise of obtaining EXAFS on the timescale of milliseconds in a single shot, it had, until very recently [15,16,18], failed to deliver. There are numerous reasons for this, some of which will be discussed below, but principal amongst these has been the provision of adequate detectors.

As such, in our first demonstration of the current experiment [9] detector readout limitations imposed upon us the collection of dispersive EXAFS and IR data on a timescale of a few seconds. Since then two solutions to this particular problem have arisen: XSTRIP, developed at CLRC Daresbury [23]; and, developed at the ESRF, the Fast Readout Low Noise (FReLoN) detector. With the implementation of this latter detector system for dispersive EXAFS [14] on ID24, restrictions on spectral repetition rates have been essentially eliminated (to the ca. 2 ms level) and we may now use this new experiment in the manner for which it was originally intended.

In this report, therefore, we demonstrate the synchronous application of EDE, DRIFTS, and mass spectrometry to the understanding of a gas–solid interaction on a timescale of a few tens of milliseconds (that of NO and H_2 interacting with Rh supported upon γ-Al_2O_3 at 573 K), and discuss the potential and limitations of this new approach to studying gas–solid processes.

2. Experimental

Synchronous EDE/IR/MS experiments were carried out at the Rh K edge on ID24 at the ESRF using a Si[3 1 1] polychromator mounted in Bragg configuration and utilising a 14 bit ADC FReLoN CCD detector system [14]. Transmission EDE experiments were made synchronously with DRIFTS. The latter were performed at 4 cm^{-1}/64 ms energy/time resolution using a Digilab FTS 7000 spectrometer and a linearized high sensitivity MCT detector. A custom built DRIFTS cell (see below) was used in conjunction with standard (Spectratech) optics. The two techniques could be synchronised to yield sampling rates for each spectroscopy of ca. 64 ms whilst a quadropole mass spectrometer continuously measured the composition of the gas phase. All gases we passed through the cell under mass flow control and, in the case of the He, an inline oxygen/moisture trap (Agilent) was placed prior to the mass flow controller. Gases were switched between cell and bypass using four port microelectric switching valves (Valco).

Five weight percent Rh samples, derived from wet impregnation of $RhCl_3{\cdot}3H_2O$ on γ-Al_2O_3 (Degussa, Alon-C), were synthesised as previously described [9,12–14,16,17]. Ca. 30–40 mg of sieved (90 μm < particle diameter < 120 μm fraction) sample was loaded into the DRIFTS/EDE/MS cell to yield an effective bed density of ca. 0.75 g cm^{-3}. Samples were then purged with He, heated to 573 K under 5% H_2/He (50 ml min^{-1}). They were then briefly reoxidised under 50 ml min^{-1} 5% O_2/He, (to remove any adventitiously adsorbed carbon species) before re-reduction under the 5%H_2/He feed. The appropriate sample temperature was then selected, and the gas flow was briefly switched back to He, before switching to 5% NO/He (50 ml min^{-1}) from a bypass. DRIFTS/EDE/MS data was then collected during between 50 and 120 s of exposure. Reduction of the NO exposed Rh under 5% H_2/He was then monitored through a further switch to He and then to the reductive gas flow (50 ml min^{-1}) whilst, again, the system was constantly monitored using DRIFTS/EDE. Calibration of EDE data was achieved using a room temperature Rh foil. Data reduction and analysis were carried out using PAXAS [24] and EXCURV [25].

2.1. The experiment: design considerations and implementation

One of the prime considerations in designing a multi-technique experiment is that none of the applied techniques are unduly compromised by the experimental geometry that must be adopted to accommodate them. The current case, a fusion of transmission based EDE and DRIFTS, is ideal in this sense: one need not interfere at all with the geometric requirements of either experiment and they can be simultaneously applied in a mutually orthogonal manner.

A schematic of the experimental arrangement is shown in Fig. 1. The overall design philosophy, from a DRIFTS perspective, follows directly from that published by Dr.

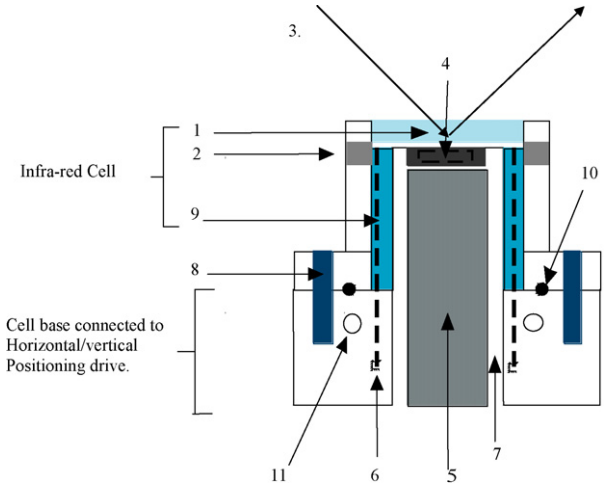

Fig. 1. Cross-sectional plan of the cell constructed and implemented for the synchronous acquisition of DRIFTS, MS, and transmission based X-ray probes under conditions of variable temperature and controlled gas flow. (1) CaF_2/ZnSe window (13 mm diameter × 2 mm); (2) 0.5 mm thick boron nitride windows/sample holder glued into sides of cell for X-ray transmission; (3) path of reflected IR light (orthogonal to X-ray path); (4) boron nitride sample cup (0.5 mm thick × 5 mm diameter × 3 mm deep); (5) cartridge/cable heater; (6) pipelines for gas feed in/out/mineral insulated type K; (7) stainless steel sample post (onto which sample is placed); (8) retaining bolts for cell; (9) volume reducing ceramic insert with conduits for gas flow/thermocouple; (10) Kalrez 'o' ring; (11) water cooling in base; (12) mounting to micrometer drive for sample height adjustment.

Gordon McDougall et al. from the University of Edinburgh [26]. The cell uses a single flat IR window (CaF_2 or ZnSe (Crystran)) rather than two windows posed at 45° to the top of the sample bed. This is done to two effects. The first is that it permits, together with the implementation of a macor insert between the sample mount and the external walls of the cell, a considerable diminution of the dead volume in the closed cell. The second is that upon closure of the cell the 0.5 mm diameter mineral insulated thermocouple (Thermocoax) used to measure the sample temperature is automatically pushed into and retained in the sample bed, the top of which is 0.5 mm below the base of the window. The base of the cell is sealed using a Kalrez 'o' ring. Using this configuration experimentation is currently possible up to ca. 673 K.

To effect X-ray transmission all that is required of the experiment is that the DRIFTS sample cup be made X-ray transmissive, and that two suitably X-ray transparent windows be incorporated into the body of the DRIFTS cell. In this case the sample cup comprises a pyrolytic boron nitride (BN) ring (Goodfellow). For experimentation at Rh K (23.2 keV) the dimensions of the sample bed were 5 mm i.d., 6 mm o.d., 3 mm depth, though sample cups of between 3 and 8 mm diameter can be accommodated. This is mounted (using a ceramic adhesive—AREMCO 471) onto a hollow stainless steel mount that slips over a central post beneath which is contained the cell heating element. Sample exchange is therefore facile and rapid.

Into the walls of the stainless steel DRIFTS cell 10 m × 3 mm apertures were machined such that windows (either hot pressed BN or kapton) could be glued using a high temperature epoxy such as araldite. Experimentally is noted that at softer X-ray energies (for instance, Pt L3 or Re K at station 9.3, CLRC Daresbury [27]) a visible broadening of, for instance, XANES could be observed when using the hot pressed BN windows. This is ascribed to the microstructure of this form of BN causing unwanted dispersion of the transmitted beam. At the higher energies required for experimentation at Rh and Pd K edges, however, this effect is found to be insignificant.

A second prime consideration of the experiment is that both the EDE and the DRIFTS spectroscopies sample, as best as is possible, the same area of the catalyst bed. As this experiment utilises a loosely packed powder as a sample, rather one that is compressed (such as a pressed disk), we are not overly concerned about the permeability of the gas throughout the bed and the potential for concentration gradients to form during experimentation. However, in order to have the greatest confidence in the results obtained this should not be ignored. Practically speaking this means that the EDE measurements should be made within (at most) the top 500 μm of the sample bed, this being the order of maximum penetration of IR light in this sort of experimental configuration and in the sorts of materials under study.

Geometrically this is easy to arrange with correct positioning of the windows in the sides of the DRIFTS cell. This does, however, place a constraint on the dimensions of the X-ray beam utilised. In the current case, as the intrinsic vertical focus of the beam on ID24 is of the order of only 100–150 μm, this is easily accommodated from an EDE perspective.

3. Results and discussion

3.1. A note on sample normalisation

Dispersive EXAFS suffers from a weakness that lies in the normalisation of the absorption spectrum obtained. To this day "in line" and synchronous normalisation of the data, as is standard with other XAFS variants, has not been demonstrated, and a separate "I(o)" must be taken. Fig. 2 shows Rh K edge EDE spectra taken one after another under flowing 5% H_2/He at 300 K and utilising two separate types of I(o). Each spectrum is the accumulation of 10 × 6 ms spectra, i.e. 60 ms total time.

The first I(o) (top spectrum (A)) simply moves the sample out of line of the beam and the X-ray pass through air. This is the most facile manner in which to obtain a background for an EDE measurement and, by and large, this has been the manner in which reference measurements have been achieved.

The second (bottom) spectrum (B) results from using a second BN sample holder mounted elsewhere on the apparatus and filled with a reference material (in this case a 0.5 wt.% Pt/Al_2O_3 catalyst) pre-treated treated and sieved in the same manner as the sample itself.

It is clear that the second method of normalisation is considerably superior to the first. Structure in the spectrum, that fails to normalise when using air as an I(o), is, largely eliminated using the dummy sample. Furthermore, though not shown, the analysable data length is considerably increased (from ca. $k = 12$ to 14.5) for the same photon flux and integration time.

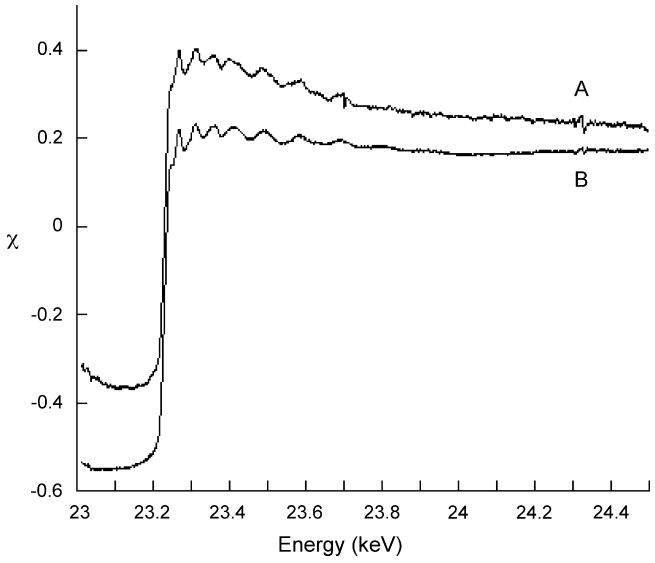

Fig. 2. The effects of different modes of normalisation of the EDE experiment. The figure shows raw Rh K edge EDE data obtained with (A) and air I(o), and (B) utilising a dummy sample (see main text). The two spectra were taken sequentially on the same sample maintained under flowing 5% H_2/He at 300 K. Each spectrum is comprised of an accumulation of 10 spectra, each having 6 ms acquisition time.

The predominant reason for this is that the dummy sample effectively mimics the homogeneity and the microstructure of the sample. As we have mentioned above an unwanted ramification of a highly coherent source, such as that found at the ESRF, is that SAXS structure derived from the sample or windows can arise and be transmitted directly to the detector. Even a hypothetical method for in line and synchronous normalisation in EDE will do nothing to counteract these effects as they arise from the sample itself. As such an effective I(o) needs to mimic both the packing and overall homogeneity of the sample but, more than that, needs to mimic the microstructure of the sample, particularly the support material, that is largely responsible for the SAXS and other scattering effects.

At least in this case, it is clear that by employing such a dummy sample that we can succeed to a considerable degree in mimicking the unwanted effects of the physical nature of the sample. As a result, the potential of the experiment for obtaining structural data is considerably improved. It must be stated, however, that these samples having a combination of a relatively hard edge—Rh K and a relatively light support material (Al_2O_3) are by no means the most challenging of samples in terms of such effects. As such to what degree this methodology may be applied in more challenging circumstances is, therefore, still open to question.

3.2. The oxidation/reduction of 5 wt.% Rh/Al_2O_3 using NO and H_2 at 573K

Fig. 3a and b show Rh K edge EDE (in k^3 and Fourier Transform (FT) forms, respectively) derived from 5 wt.% Rh samples maintained under: (A) flowing 5% H_2/He; (B) He; (C) after 50 s exposure to 5% NO/He at 573 K; (D) after 50 s exposure to 5% H_2/He; and (E) after re-reduction under flowing 5% H_2/He. Structural and statistical data arising from analysis of these data are given in Table 1.

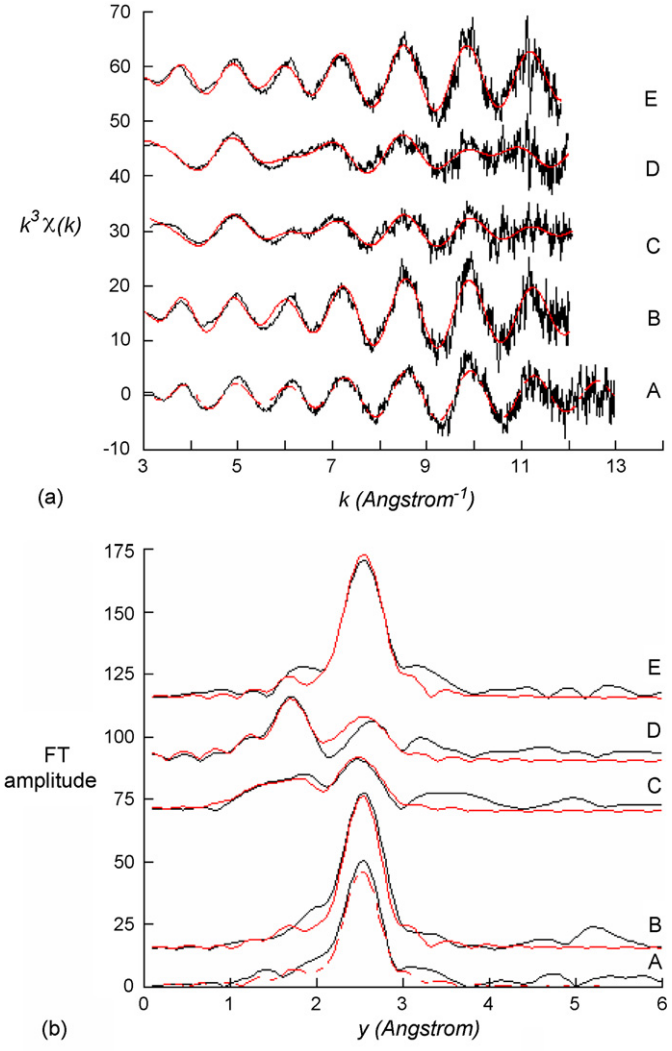

Fig. 3. Rh K edge EDE spectra, shown in k^3 (a) and FT (b) forms, derived from a 5 wt.% Rh sample maintained under: (A) 5% H_2/He; (B) He; (C) after 50 s exposure to 5% NO/He (sample still under He); (D) after a further 50 s exposure to NO but maintained under He just before a switch to 5% H_2/He; (E) under 5% H_2/He after 50 s exposure. Spectral acquisition time in each case was 62 ms, the sample temperature was 573 K.

At 573 K under both H_2 and He environments the EDE indicates the retention of an fcc nanoparticulate structure as expected. However, the first shell Rh–Rh co-ordination number indicated from analysis is only ca. 4.5 rather than the figure of ca. 7 generally expected for these samples [9,12–15,17]. A more extensive discussion of this observation is given elsewhere [28]. It appears that, between 473 and 573 K, Rh nanoparticles appear to shrink/spread over the Al_2O_3 dispersant to a significant degree. In the simplest approximation, assuming a constant (hemispherical) morphology [29] and fcc structure, and in the absence of significant asymmetry in the Rh–Rh pair distribution function [28,30], a change in the average particle size from ca. 35 to 40 atoms (11 Å diameter), to around ca. 10–15 atoms (8 Å diameter), is indicated between these temperatures.

Table 1
Structural and statistical parameters derived from the dispersive EXAFS spectra shown in Fig. 3 after reduction using PAXAS and [24] analysis using EXCURV [25]

Spectrum	Atmosphere/experiment	k_{min} (Å^{-1})	k_{max} (Å^{-1})	Scatterer	CN	r (Å^{-1})	DW ($2\sigma^2$)	E_F (eV)	R (%)
A	5% H_2/He	3	13.00	Rh	4.4	2.635	0.018	−0.8	48.7
B	He	3	12.00	Rh	5.0	2.640	0.016	0.6	44.9
C	5% NO/He, after 50 s exposure	3	12.00	Rh	1.7	2.650	0.015	1.9	51.8
				O	1.9	2.059	0.010		
				N	0.8	1.877	0.009		
D	After 2 × 50 s, NO/He, under He	3	12.00	Rh	1.5	2.655	0.014	1.5	62
				O	2.2	2.027	0.006		
				N	0.8	1.830	0.007		
E	After 50 s 5% H_2/He, under H_2/He	3	12.00	Rh	4.9	2.645	0.017	−0.46	45.2

Errors in CN should be considered in the range ±10–20%, those of bondlengths (r) ± 1.5–2%, R (%) = ($\int[\chi^T - \chi^E]k^3\,dk/[\chi^E]k^3\,dk$) × 100%: χ^T being the theoretically calculated EXAFS and χ^E being the EXAFS obtained via experiment. σ = the root mean square displacement in internuclear separation.

Exposure of these reduced Rh particles to NO at 573 K for 50 s oxidises the Rh to a considerable extent (spectrum C in each figure) and the formation of an $Rh_xO_yN_z$ phase is indicated. Complete oxidation/formation, however, does not occur within this time frame as shown by spectrum (D) obtained after a further exposure to NO for 50 s followed by flowing He. It should be noted that in a bulk Rh_2O_3 type system a Rh–Rh CN of 2 is expected at ca 2.71 Å with a corresponding low Z CN (in this case of N or O) of 3.

Subsequent exposure of the reduced catalysts to 5% H_2/He restores the Rh to an fcc nanoparticulate form with no evidence for any increased net particle size (i.e. from the Rh–Rh CN) that one might expect if sintering processes were active at this temperature and on these timescales.

Analysis of the data derived from the mass spectrometer for the interaction of the NO with the sample during the first 50 s of NO exposure indicates a NO uptake of ca. 1.4 (±0.2) NO/Rh with a net selectivity to $N_{2(g)}$ (as opposed to N_2O_g) of ∼55%. Given that each N_2 and N_2O molecule produced to the gas phase implies the formation of 2 and $1O_{(a)}$, respectively, and that these remain associated with the Rh, a level of oxidation of ca. $RhO_{1.2}$ is implied at this point.

Fig. 4 shows representative infrared spectra taken concomitantly at 573 K with the EDE and MS and at 16 Hz (64 ms) spectral repetition rate. These show, spectra after 50 s NO exposure, but still under flowing 5% NO/He (A), post-NO exposure but after having returned to a He flow (B), and the difference between the two (C). The position and relative intensity of bands expected from $NO_{(g)}$ [31] are indicated above spectrum (C). In both instances exposure of the NO oxidised samples to 5% H_2/He results in the removal of all NO functionality within 50 s.

The spectra derived after exposure to NO are dominated by the presence of a linear Rh(NO^+) species at 1911 cm^{-1} [32]. Under flowing 5% NO/He other functionality is indicated to be present in the range 1500–1750 cm^{-1}. This may be derived from a number of species but, given the level of oxidation of the Rh indicated from the EXAFS at this point (see above), we would assign the species at ca. 1500–1650 cm^{-1} as being due to nitrates formed either on the oxidised Rh phase or on the support [32,33]. The bands appearing above between 1700 and 1750 cm^{-1} could have their origin from the asymmetric stretch of an $Rh(NO)_2$ species or from a "high wavenumber $Rh(NO)^-$ species" [34–37]. Unfortunately, the weaker symmetric stretch of the $Rh(NO)_2$ species is expected at 1825 cm^{-1} [35] and is therefore extremely difficult to deconvolute from gas phase NO contributions (indicated in the difference spectrum (C)). As such a verification of its presence or absence at this temperature is not directly possible. When 5% NO/He is replaced by flowing He (spectrum (B)) the only feature indicated to remain on the catalyst is the linear Rh-nitrosyl (1911 cm^{-1}).

Fig. 5 shows the temporal changes observed in the Rh K edge XANES along with those observed for the Rh(NO^+) species in DRIFTS during oxidation by NO and subsequent

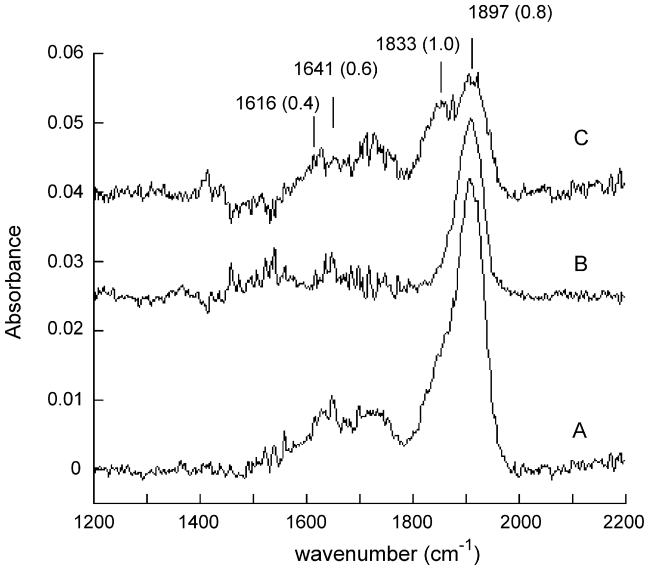

Fig. 4. DRIFTS spectra obtained from an initially reduced 5 wt.% Rh sample after: (A) 50 s exposure to 5% NO/He at 573 K and still under 5% NO/He; (B) post-NO exposure under flowing He at 573 K. Spectrum C shows the difference between spectra (A and B). The expected positions and relative intensities of bands expected from $NO_{(g)}$ are indicated.

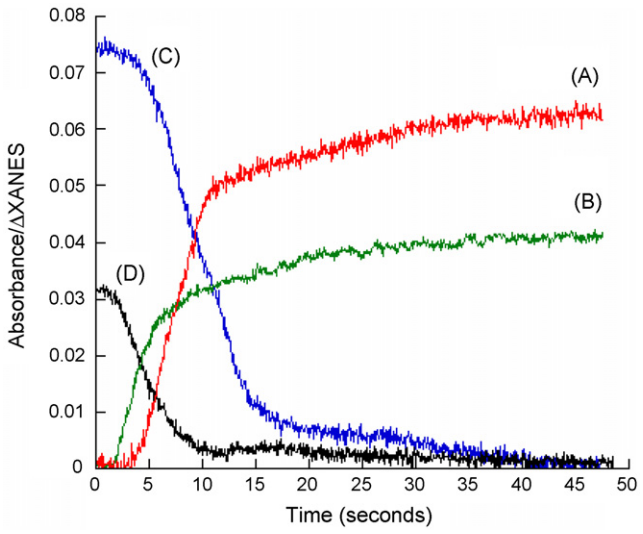

Fig. 5. The synchronously measured temporal variations observed Rh K edge XANES and at 1911 cm^{-1} in DRIFTS for the oxidation/reduction of 5 wt.% Rh/Al_2O_3 at 573 K. (A) XANES during NO exposure; (b) DRIFTS during exposure to NO; (c) XANES during exposure of NO reacted sample to 5% H_2/He; (D) during exposure of NO reacted sample to 5% H_2/He. The changes in XANES were calculated taking the raw difference in absorption between the measured absorption at 23.235 and 23.237 keV.

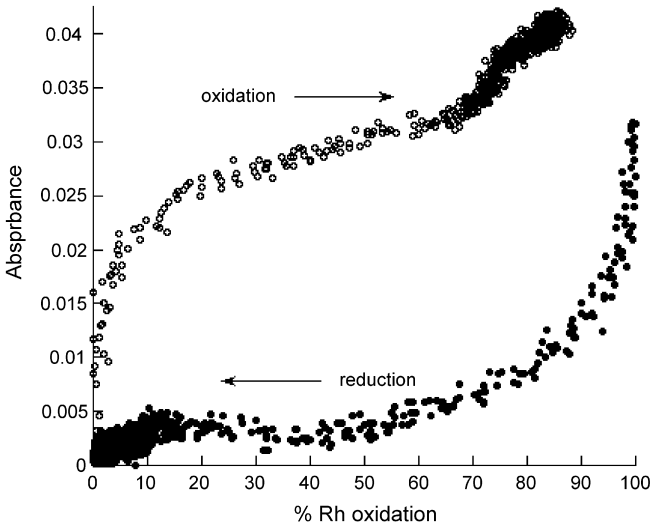

Fig. 6. The correlation, obtained at 573 K, between the appearance (under 5% NO/He) and removal (under 5% H_2/He), of the linear nitrosyl functionality observed at 1911 cm^{-1} in DRIFTS, with the degree of Rh oxidation indicated from dispersive XANES and EXAFS measurements. Each experiment last 50 s with DRIFTS measurements made every 64 ms, and EDE every 62 ms. 100% Rh oxidation is assumed to result in a Rh 3+ system of the stoichiometry Rh_2O_3—see text.

reduction using 5% H_2/He at 573 K. From the viewpoint of the XANES the oxidation by NO shows two clearly distinct regimes, the second much slower than the first. Such a two stage process is not evident at all in the appearance of the linear nitrosyl species. Moreover, the formation of this species in DRIFTS is seen occurring in advance start of the structural change indicated by the XANES.

For the most part the reduction of the oxidised phase formed under NO can be seen as occurring in a single step though the last 20% of the changes seen in XANES do appear to proceed at a tangibly lower rate, possibly indicative of a second step in the reduction process. As with the oxidation however, it also appears that the removal of the NO^+ species precedes the vast majority of the reduction indicated from XANES.

The variation in the XANES, together with analysis of the EXAFS obtained during this process permits an assessment of how the variation in functionality is related to the degree of oxidation of the Rh phase. Fig. 6 shows this as a correlation plot between the intensity of the NO^+ species versus percentage oxidation of the Rh phase. This shows even more clearly the apparently different temporal relationship between the growth/diminution of the nitrosyl functionality and the degree of oxidation and phase of the Rh.

The % level of Rh oxidation is derived with the assumption that the most oxidised state that can be achieved under these conditions is Rh_2O_3. This is justified on the basis of previous work using O_2 as an oxidant [17] and, in this case from the net uptake (not shown) of NO realised during an experiment (measured using MS) which, at most = 1.6NO/Rh [37,38].

It is clear that at 573 K a significant amount of NO^+ functionality is formed before the onset of a significant amount of oxidation. Conversely significant reduction of the oxidised Rh phase appears to only be possible after the removal of the $Rh(NO^+)$ species.

From the data shown above it can be deduced that the $Rh(NO^+)$ species is essentially stable toward decomposition/desorption under flowing He at 373 K. That a significant proportion of this species can form prior to the observation of a large amount of Rh oxidation would imply that some sites capable of supporting this species are already present in the system, most likely Rh particle/Al_2O_3 interfacial sites. Thereafter, the NO^+ formation follows the two stages of oxidation indicated in Fig. 5.

We would therefore take the view that this species occupies interface/defect sites associated with oxidised Rh, but that is it does so after these sites are formed, rather than being actively involved in their formation. This would be consistent with the notion that such a nitrosyl species acts as an electron donor to the Rh phase that supports it. As such it will not form on electron rich (for instance, reduced) phases of Rh but can act to stabilise electron deficient phases. Such phases will be found at metal/oxide interfaces, at the periphery of supported nanoparticles, or within a nascent oxide layers growing through reactive (dissociative) NO adsorption.

That the NO^+ species appears to be removed to facilitate subsequent reduction of the Rh oxide phase makes sense within this idea as its presence most likely blocks the types of surface site required to initiate H_2 dissociation and therefore promote reduction. Though this reduction is visibly rapid, what remains to be divined is exactly how this initial reaction/displacement of the NO^+ species occurs: molecular NO production is not observed in the MS, and both MS and IR are inconclusive as to the transient formation of protonated nitrogen species.

Fig. 7 shows the relationship between the functionality observed in IR at 1745 cm^{-1} and the net selectivity observed in

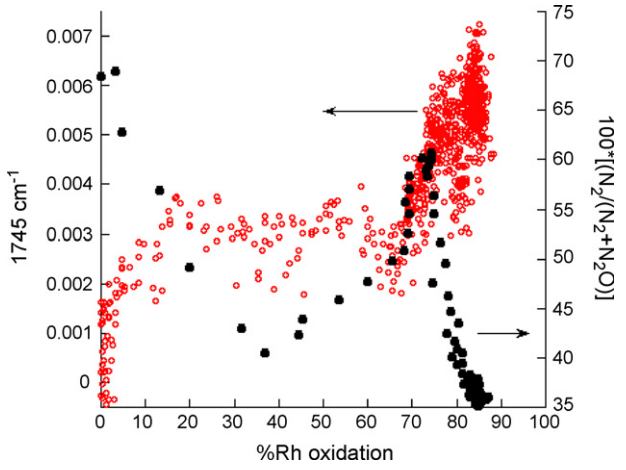

Fig. 7. Correlation between the selectivity toward N_2 ($100 \times [N_{2(g)}/(N_{2(g)} + N_2O_{(g)})]$)—red (○), and infrared functionality observed at 1745 cm^{-1}—black (●), with the degree of oxidation of the Rh phase attained during exposure of reduced 5 wt.% Rh samples to 5% NO/He for 50 s at 573 K. Again, 100% Rh oxidation is assumed to result in a Rh 3+ system of the stoichiometry Rh_2O_3—see text. (For interpretation of the references to colour in this figure legend, the reader is referred to the web version of the article.)

the gas phase during the exposure of NO to reduced Rh nanoparticles at 573 K. This is shown as a function of the degree of oxidation of the Rh derived from analysis of the XANES and EXAFS taken concurrently.

The initial interaction of NO with reduced Rh is highly selective for the formation of N_2. This initial selectivity rapidly diminishes as oxidation proceeds between 30 and 50% oxidation. A transient recovery of N_2 selectivity is then observed up to ca. 70% Rh oxidation. Thereafter, a rapid decline in both NO turnover (not shown) and the selectivity of the interaction toward N_2 ensues as the oxidic Rh phase becomes ever more complete. This latter observation is consistent with our previous work on these systems [13]. The persistence of a highly oxidised Rh phase in this temperature regime, under NO rich, NOH_2, feedstocks [13], leads to a low NO turnover (forming N_2O rather than N_2) that diminishes to 0 above 600 K.

It is clear that, at 573 K a considerable correlation exists between the IR peaks at 1911 and 1745 cm^{-1} and the selectivity of the interaction. However, for the reasons outlined above, regarding the reactivity of the NO^+ species, and a more extensive survey of the temperature dependence of this interaction given elsewhere [38], it is the latter species that we associate with most of the reactive oxidation of the Rh and the N_2O production observed both at lower temperatures and at intermediate levels of Rh oxidation.

As mentioned, however, this band may have more than one origin, i.e. the so called "high wavenumber NO^- species" and the Rh geminal dinitrosyl ($Rh(NO)_2$) species. Contributions from NO_g to the IR spectrum around 1825 cm^{-1} make it virtually impossible to state unequivocally, in this instance, whether this latter species is present. Intuitively the geminal dinitrosyl can only yield N_2O as a decomposition product and, therefore, it alone cannot explain the selectivity achieved during the greater part of this interaction. The simplest explanation of the observations is that a bent mononitrosyl, that can only form at the interface between oxidised and reduced Rh, is responsible for most of the observed oxidation and reactivity chemistry observed [38].

Within this framework the only observation that cannot adequately be explained is the precipitous drop in selectivity observed at >70% Rh oxidation. This point also corresponds to the inflection in the rate of Rh oxidation observed at ca. $t = 11$ s and is interpreted as indicating the completion of an oxidised layer, or fraction of layer, beyond which further oxidation is controlled by penetration of oxygen into the remainder of the Rh particle.

As this further penetration of the particles occurs the defect sites resulting can be filled by forming a $Rh(NO^+)$ species. This results in a slow increase (as is seen) in the population of this species but, in the absence of another decomposition route, would stop any further oxidation (we have already noted that the NO^+ species under an inert environment appears to be stable at 573 K).

That oxidation does not stop, but continues at a much reduced pace under NO indicates that there has to exist a second path for advancing Rh oxidation and, at the same time, one that promotes the formation of N_2O. Clear evidence for this can be found in the MS in that two distinct phases of N_2O production are observed at this temperature shown in Fig. 8. The first is active between 10 and 70% Rh oxidation and is responsible for the broad minimum in selectivity observed therein. Above 75% Rh oxidation, the second stage of N_2O production becomes evident and, as the total rate of N_2 production is falling rapidly by this time, selectivity to N_2 drops accordingly. The brief recovery of selectivity to N_2 between 50 and 75% oxidation represents the junction between these two phases where the first has essentially finished, the second is only starting to augment with the surface concentration of $Rh(NO^+)$. As such it is at this point that we invoke the participation of transient $Rh(NO)_2$

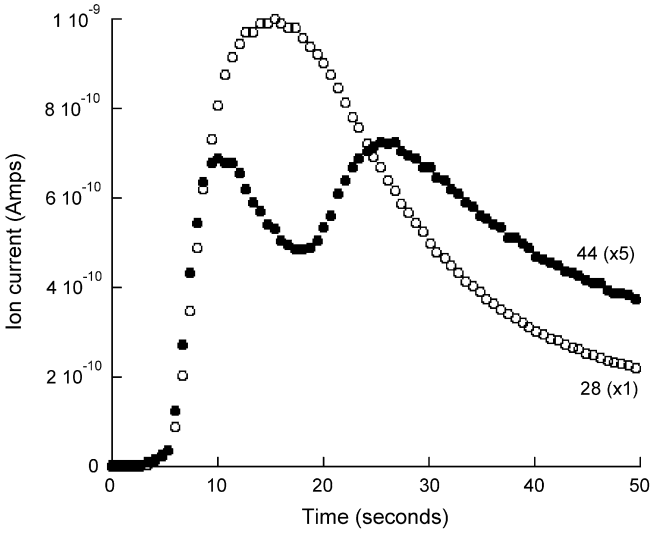

Fig. 8. Temporal responses of mass 28 ($N_2 + N_2O$; open circles) and mass 44 (N_2O; filled circles) observed during reaction of reduced 5 wt.% Rh/Al_2O_3 at 573 K with 5% NO/He. The presence of two distinct phases of N_2O production are apparent.

species as has been proposed previously [34–37] in these systems.

3.3. Limitations/potential of the methodology

Above we have given a general description and an example of the application of this new experiment to a particular system. However, as no single experiment is a panacea, it is worth considering the limitations that exist, and how some of these might be circumvented and/or improved. In doing so we will concentrate on the limitations imposed on X-ray based experiments (such as EDE) and the DRIFTS cell itself with the implicit assumption that the other components of the system are not unduly undermined by the required experimental geometry (see above). In some cases hard and fast rules regarding the applicability of the experiment cannot be given as they arise from the interplay of a number of factors. But the following is, however, given as a guide.

As the experiment is transmission based finite constraints exist on the diameter of the sample beds used. Investigation using increasingly soft X-rays, or indeed, increasingly absorbing support materials, will require an ever diminishing path length through the sample. Whilst this can be easily accommodated (down to ca. 1 mm path length through the sample bed) this starts to cause problems for the DRIFTS part of the experiment (using standard optics). At present, we have succeeded in obtaining data for 1–5 wt.% Re L_{III} and Pt L_{III} samples supported upon Al_2O_3 and SiO_2 [27] using 3 mm diameter sample beds. With a 3 mm it has also been possible to obtain a suitable alignment for the infrared component of the experiment.

As a rule of thumb therefore, with the current configuration, transmission EXAFS experiments at around 11 keV could be regarded as a practical limitation to the applicability of this experiment for systems of this sort of metal loading and support combination. Extending the range of this sort of synchronous XAFS/FT-IR experiment, to encompass for instance the first row transition metals, requires a different methodology, based upon another form of IR experiment (for instance, transmission, or possibly ATR [5]). However, this general assessment needs to be further modified to take into account the nature of the support material. For example, whilst the study of Au supported on Al_2O_3 or SiO_2 appears possible at the Au L_3 edge [27] studying the system catalytic preference, i.e. Au/TiO_2, is not proved possible. Similarly, experimentation on, for instance, Pt based auto exhaust catalysts, that typically contain low levels of Pt combined with elements such as Ce, Zr, B, La within the support material, will not be possible, whereas, at least from an X-ray transmission point of view, the behaviour of Rh and Pd components should be amenable to the technique.

It is clear from the results shown here that for elements such as Rh very good dispersive EXAFS data can be achieved at the 5 wt.% Rh level. We have also obtained analysable EXAFS data at the 2 wt.% Rh level [39], on similar timescales, using the same sample beds. Again, however, what one may obtain is also a function of the nature of the support material and normalisation methodology. The current data, along with data previously obtained from ID24 from similar systems [14,16] would suggest that the reasonable limit for dynamic, single shot, XANES (and possibly EXAFS) studies on heterogeneous systems of this type would be at ca. 1 wt.% metal loading.

At present, the heating capacity of the cell is also limited to ca. 673 K. There are two reasons for this. The first is that the heating mechanisms used to date are somewhat indiscriminate in their delivery of power. The second is that the drive for minimising the internal volume of the system (that was, in the first instance, for time resolved studies considered to be most important), necessarily means that the IR windowing is brought very close to the sample itself. The nature of the windowing materials (CaF_2 or ZnSe) means that they are both difficult to cool evenly and that they have a propensity to crack or otherwise degrade at temperatures much in excess of this. Though new solutions to these problems are being studied at the ESRF, for the moment it seems that some form of trade off between the minimisation of internal dead volume and the ultimate temperature of usage will persist. At the ESRF we are currently implementing a modified commercial DRIFTS cells for this experiment. These have an intrinsic capacity to work to temperatures of ca. 1000 K though they do this through using IR windows canted at 45° to the sample. This necessarily introduces a dead volume that is not easily eradicated. However, we can anticipate that XANES/EXAFS/DRIFTS experiments at these more elevated temperatures (and potentially elevated pressures) will soon be possible.

Moreover, we also anticipate that, as this experiment is based around the generic notion of X-ray transmission, it should be able to be utilised for standard and Quick EXAFS along with diffraction variants such as SAXS and WAXS providing the dimensions of the X-ray beam conform to the requirements outlined in Section 2.

4. Summary and conclusions

We have successfully demonstrated a new methodology for simultaneously addressing structure (in this instance using dispersive XAFS), functionality (using DRIFTS), and reactivity (MS) at high time resolution. This experiment is well suited to the study of the dynamic behaviour of solids (in powder form), and gas–solid interactions, though certain provisos regarding the absorption of the material itself and the hardness of the X-rays required do not make the experiment globally applicable (for instance, to first row transition metals in XAFS).

Where applicable, however, it does permit a currently unique insight into the relationships between structure, function and reactivity for systems and processes that are relatively fast (occurring on the timescale of a few seconds of below).

The application of this technology to the study of the oxidation (by NO) and reduction (by H_2) of supported Rh reveals new insights into the details of how such fundamental interactions proceed. For instance, we have isolated, the specific role that the linear NO^+ species has in both oxidation and reduction of Rh, and the role it may play reactively at elevated temperatures, whilst directly gaining new information to its physical character and the nature of the Rh phase/sites

with which it is associated. We have been able to assess the rates at which it is formed and removed, whilst at the same time as assessing how the structures that support it are changing.

As such, using a prototypical model of the chemistry of Rh in auto exhaust catalysis we hope to have demonstrated a considerable potential for the quantitative braiding of dynamic structural, reactive, and functional behaviour in a single experiment.

Acknowledgements

This work was funded by the EPSRC UK (Grant Number GR/60744/01) and the authors thank the EPSRC for the provision of postdoctoral and Ph.D. funding to MAN and BJ, respectively. The ESRF are thanked for the provision of facilities within a long term proposal awarded for this research. John James (University of Southampton), and Florian Perrin (ESRF) are gratefully acknowledged for their technical contributions to this work. Dr Gordon McDougall is also greatly thanked for the technical schematics of a novel DRIFTS cell designed and constructed at the department of chemistry, Universiy of Edinburgh, Scotland. MAN would further like to thank the directors of the ESRF for funding for the continued development and implementation of this methodology at the ESRF for the wider use of the scientific community.

References

[1] For instance, B.M. Weckhuysen, PCCP, 5 (2003) 4351.
[2] B.S. Clausen, H. Topsøe, R. Frahm, Adv. Catal. 42 (1998) 315.
[3] G.S. Sankar, J.M. Thomas, Top. Catal. 8 (1998) 1.
[4] (a) J.G. Mesu, A.M.J. van der Eerden, F.M.F. de Groot, B.M. Weckhuysen, J. Phys. Chem. B 109 (2005) 4042;
(b) S. Diaz-Moreno, D.T. Bowron, J. Evans, Dalton Trans. 23 (2005) 3814;
(c) G. Guilera, M.A. Newton, C. Polli, S. Pascarelli, M. Guino, K.K. Hii, Chem. Commun. (2006) 4306.
[5] A.M. Beale, A.M.J. van der Eerden, K. Kervinen, M.A. Newton, B.M. Weckhuysen, Chem. Commun. (2005) 3015.
[6] V. Briois, D. Lutzenkirchen-Hecht, F. Villain, E. Fonda, S. Belin, B. Griesebock, R. Frahm, J. Phys. Chem. A 109 (2005) 320.
[7] J.D. Grunwaldt, A. Baiker, PCCP 7 (2005) 3526.
[8] J.D. Grunwald, M. Ramin, M. Rohr, A. Michailovski, G.R. Patzke, A. Baiker, Rev. Sci. Instrum. B 76 (2005), Art. No. 054104.
[9] M.A. Newton, B. Jyoti, A.J. Dent, S.G. Fiddy, J. Evans, Chem. Commun. (2004) 2382.
[10] C.T. Williams, E.K.-Y. Chen, C.G. Takoudis, M.J. Weaver, J. Phys. Chem. B 102 (1998) 4785.
[11] J. Grunwaldt, D. Lutzenkirchen-Hecht, M. Richwin, S. Grundmann, B.S. Clausen, R. Frahm, J. Phys. Chem. B 105 (2001) 5161.
[12] T. Campbell, A.J. Dent, S. Diaz-Moreno, J. Evans, S.G. Fiddy, M.A. Newton, S. Turin, Chem. Commun. (2002) 304.
[13] M.A. Newton, A.J. Dent, S. Diaz-Moreno, S.G. Fiddy, J. Evans, Angew. Chem. Int. Ed. 41 (2002) 2587.
[14] M.A. Newton, B. Jyoti, A.J. Dent, S. Diaz-Moreno, S.G. Fiddy, J. Evans, Chem. Phys. Chem. 5 (2004) 1056.
[15] M.A. Newton, S.G. Fiddy, G. Guilera, B. Jyoti, J. Evans, Chem. Commun. (2005) 118.
[16] A. Iglesias-Juez, A. Martinez-Arias, M.A. Newton, S.G. Fiddy, M. Fernandez-Garcia, Chem. Commun. (2005) 4094.
[17] M.A. Newton, A.J. Dent, S. Diaz-Moreno, S.G. Fiddy, B. Jyoti, J. Evans, Chem. Eur. J. 12 (2006) 1975.
[18] A. Suzuki, Y. Inada, A. Yamaguchi, T. Chihara, M. Yuasa, M. Nomura, Y. Iwasawa, Angew. Chem. Int. Ed. 42 (2003) 4795.
[19] For instance, J.T. Gleaves, J.R. Ebner, T.C. Kuechler, Catal. Rev. Sci. Eng. 30 (1988) 49.
[20] For example, K. McFarlane, B. Lee, J. Bridgewater, P.C. Ford, J. Organomet. Chem. 554 (1998) 49.
[21] For example, M.A. Newton, A.J. Dent, J. Evans, Chem. Soc. Rev. 31 (2001) 83.
[22] M. Richwin, R. Zaeper, D. Lutzenkirchen-Hecht, R. Frahm, Rev. Sci. Instrum. B 73 (2002) 1668.
[23] G. Salvini, J. Headspith, S.L. Thomas, G. Derbyshire, A. Dent, T. Rayment, J. Evans, R. Farrow, S. Diaz-Moreno, C. Ponchut, Nucl. Instrum. Methods A 551 (2005) 27.
[24] N. Binsted, PAXAS: Programme for the Analysis of X-ray Adsorption Spectra, University of Southampton, 1988.
[25] N. Binsted, EXCURV98, CCLRC Daresbury Laboratory Computer Programme, 1998.
[26] See, for example,
(a) I.R. Harkness, M. Cavers, L.V.C. Rees, J.M. Davidson, G.S. McDougall, in: B.K. Marcus, M.M.J. Treacy, J.B. Higgins, M.E. Bisher (Eds.), Proceedings of the 12th International Zeolite Conference, vol. IV, Materials Research Society, Warrendale, PA, 1999, p. 2615;
(b) M. Cavers, J.M. Davidson, I.R. Harkness, G.S. McDougall, L.V.C. Rees, in: G.F. Froment, K.C. Waugh (Eds.), Reaction Kinetics and the Development of Catalytic Processes, vol. 122, Elsevier, Amsterdam, 1999, p. 65.
[27] B. Jyoti, M.A. Newton, S.G. Fiddy, A.J. Dent, J. Evans, I. Harvey, unpublished data.
[28] M.A. Newton, A.J. Dent, S.G. Fiddy, B. Jyoti, M. Tromp, J. Evans, in preparation.
[29] A. Jentys, PCCP 17 (1999) 4059.
[30] For example:
(a) B.S. Clausen, J.K. Norskov, Top. Catal. 10 (2000) 221;
(b) G.E. van Dorssen, D.C. Koningsberger, PCCP 5 (2003) 3549.
[31] http://webbook.nist.gov/cgi/cbook.cgi.
[32] H. Arai, H. Tominaga, J. Catal. 43 (1976) 131.
[33] N.D. Parkyns, J. Chem. Soc. A (1969) 410.
[34] J.A. Anderson, G.J. Millar, C.H. Rochester, J. Chem. Soc. Faraday Trans. 86 (1990) 571.
[35] J. Liang, H.P. Wang, L.D. Spicer, J. Phys. Chem. 89 (1985) 5840.
[36] R. Dictor, J. Catal. 109 (1988) 89.
[37] E.A. Hyde, R. Rudham, C.H. Rochester, J. Chem. Soc. Faraday Trans. 80 (1988) 531.
[38] M.A. Newton, A.J. Dent, S.G. Fiddy, B. Jyoti, J. Evans, Phys. Chem. Chem. Phys, in press.
[39] M.A. Newton, A.J. Dent, S.G. Fiddy, B. Jyoti, J. Evans, J. Mater. Sci., in press.